IFSCC 2025 full paper (1334)

Surface Morphology Control of Sustainable Functional Cosmetic Particles Using Green Spray Drying Process

Seoyoon Lee* [1], Seo Yeon Park[2], Hye Yun Park[2], Jihui Jang[1], Heemuk Oh[1], Sung Yun Hong[1], Chun Ho park[1],Jun Bae Lee[1], Jun Hyup Lee[2]

[1]R&I Center, COSMAX, Seongnam-si, Republic of Korea
[2]Chemical engineering, Soongsil University, Seoul, Republic of Korea

1. Introduction

Calcium carbonate ($CaCO_3$) is a naturally occurring inorganic material that has attracted significant attention as a plastic-free, sustainable and environmentallyfriendly raw material. Owing to its low cost, excellent biocompatibility, and non-toxicity, it is widely used across various industries, including food, pharmaceuticals, and cosmetics. In the cosmetics field in particular, $CaCO_3$ is commonly utilized in a variety of formulations as a buffer, opacifying agent, bulking agent, absorbent, and abrasive [1]. However, conventional $CaCO_3$ particles typically exhibit irregular, non-spherical morphologies, which can limit their applicability owing to issues such as poor spreadability and dispersion stability. In contrast, spherical $CaCO_3$ particles offer enhanced filling efficiency, higher dispersibility, and superior whiteness, making them ideal fillers and pigments in a wide range of product formulations. Specifically, spherical $CaCO_3$ particles with porous structures can provide multifunctional properties, including improved skin delivery efficiency of active ingredients owing to their high surface area, as well as enhanced light-scattering performance, hydrophobicity, and oleophobicity [2]. Although various methods for synthesizing spherical $CaCO_3$ particles have been studied, many of these processes involve high temperatures, high energy input, and complex multi-step procedures, often requiring additives or organic solvents, which present environmental and economic limitations [3,4]. Therefore, there is a growing demand for eco-friendly, simple, and energy-efficient processes for producting spherical $CaCO_3$ particles.

In this study, cellulose nanofibers (CNFs) were employed as binders to fabricate spherical $CaCO_3$ composite particles by co-aggregating and drying CNFs with $CaCO_3$ nanoparticles via a spray-drying technique. Cellulose is a biodegradable, non-toxic, and biocompatible material with broad applicability in industries such as cosmetics, food, textiles, and biomedical engineering [5]. CNFs possess abundant hydroxyl groups on their surfaces, which enable hydrogen bonding and electrostatic interactions, allowing them to act as binders, reinforcing agents, or adhesives in composite materials [6]. These physicochemical properties enable the formation of uniform spherical composite particles by inducing strong interactions with $CaCO_3$ particles and forming a three-dimensional network structure within the droplets during spray drying.

Spray drying is a continuous process that atomizes liquid feed into fine droplets and rapidly dries them through contact with hot gas. This technique enables the formation of dry powders in seconds, making it highly attractive owing to its time efficiency and energy-saving potential [7]. Moreover, spray drying omits complex steps, such as washing, filtration, and prolonged drying, improving production efficiency and allowing for cost-effective operation, which is advantageous for industrial-scale manufacturing. In particular, by adjusting spray-

drying parameters, such as feed rate and gas flow, it is also possible to precisely tailor particle size and morphology, thus enabling the design of materials with diverse functionalities.

Accordingly, in this study, we successfully manufactured spherical $CaCO_3$/CNFs composite particles in a short period of time through an eco-friendly process of dispersing $CaCO_3$ nanoparticles and CNFs in deionized water and then co-spray drying them. In particular, the porous structure of the particles was controlled by adjusting the spray drying conditions, and the composite particles produced through this were able to exhibit multifunctional performances such as improved water and oil repellency, increased particle hardness, and excellent light reflectivity. Furthermore, this process is notable for being entirely water-based and solvent-free, thereby offering significant sustainability and industrial applicability.

2. Materials and Methods

2.1. Preparation of the spray drying suspension

Calcium carbonate ($CaCO_3$) nanoparticles with a particle size of 60–100 nm and a 2 wt% aqueous slurry of cellulose nanofibers (CNFs), with widths ranging from 10 to100 nm and lengths of 1000–5000 nm, were added to deionized water. The mixture was subjected to ultrasonication at 80% amplitude for 10 min. Subsequently, to achieve uniform dispersion of the $CaCO_3$ nanoparticles and CNFs, the suspension was stirred at 800 rpm for 30 min.

2.2. Fabrication of $CaCO_3$/CNFs composite particles using spray drying

The prepared suspension was spray-dried using a laboratory-scale spray dryer (KLSD-1500, Korea Medi). Spherical $CaCO_3$ composite particles were obtained by co-spray drying $CaCO_3$ nanoparticles and CNFs in deionized water. Additionally, the morphology of the final particles was effectively controlled by adjusting the feed rate during the spray-drying process. The materials and processing parameters used are summarized in Table 1, and the effects of CNFs addition and feed rate variation on particle formation were investigated. The abbreviation "CCn" refers to the $CaCO_3$/CNFs composite particles, and the number in the sample name is assigned to distinguish each particle according to the feed rate conditions. "$CaCO_3$-n" refers to spray-dried particles composed solely of $CaCO_3$ nanoparticles without CNFs, and the number reflects the same processing condition as that of the CCn samples.

Table 1. Process and material variables of the spray drying process

Sample code	Spray drying variables			Slurry variables
	Inlet temperature (℃)	Feed rate (mL/min)	Gas flow rate (L/h)	Concentration (wt%)
CC1	135	8.3	300	$CaCO_3$ 10 CNF 0.1
CC2	135	5.5	300	$CaCO_3$ 10 CNF 0.1
$CaCO_3$-1	135	8.3	300	$CaCO_3$ 10
$CaCO_3$-2	135	5.5	300	$CaCO_3$ 10

2.3. Characterization

The morphology and size of the $CaCO_3$/CNFs composite particles were observed using field-emission scanning electron microscopy (FE-SEM; Gemini SEM 300, ZEISS). To investigate the effect of surface morphology on the optical properties of the particles, reflectance was measured in the wavelength range of 400–1400 nm using a diffuse reflectance near-infrared (NIR) spectrometer (LabSpec 4 Bench, Malvern Panalytical). The soft-focus effect of the particles was evaluated by measuring the reflected light from 0° to 180° after irradiating light at a 45° angle using a goniophotometer (Murakami Color Research Laboratory, GP-5). The repellency of the particles against water and oil droplets was evaluated using a contact angle analyzer (SEO, Phoenix MT), where the particles were coated onto a poly(methyl methacrylate) (PMMA) substrate for the experiment. The hardness of the particles was measured using a nanoindenter (NHT3, Anton).The spreadability of the particles was quantitatively evaluated by applying the sample to actual human skin, capturing images, pixelating them using ImageJ software, and converting the data into histograms to calculate the standard deviation.

3. Results

3.1. Fabrication of spherical $CaCO_3$/CNFs composite particles

$CaCO_3$ nanoparticles tend to aggregate during the spray-drying process owing to their high surface energy, often resulting in the formation of irregularly shaped and non-uniform microparticles [8]. However, when cellulose nanofibers (CNFs) are added to an aqueous suspension of $CaCO_3$ nanoparticles, effective interactions between the two components are induced through electrostatic attraction between the oxygen atoms of carbonate ions and the abundant hydroxyl groups of CNFs, enabling structural control [9]. In this study, we successfully fabricated uniformly shaped spherical $CaCO_3$/CNFs composite microparticles by utilizing the characteristics of CNFs to function as a structural framework. Figure 1(a) shows FE-SEM images of $CaCO_3$-1 and $CaCO_3$-2 samples, prepared without CNFs, and the CC1 and CC2 composite particles, synthesized using both CNFs and $CaCO_3$ nanoparticles, under two different feeding rates (5.5 and 8.3 mL/min). In the $CaCO_3$-1 and $CaCO_3$-2 samples without CNFs, random aggregation was observed due to irregular inter-particle bonding, resulting in the formation of non-spherical microparticles. In contrast, the CC1 and CC2 samples with CNFs displayed nearly perfectly spherical morphologies. This is attributed to the CNFs, which, owing to their high aspect ratio, form a three-dimensional network structure via intermolecular hydrogen bonding within the droplets and simultaneously interact strongly with the $CaCO_3$ nanoparticles. These interactions facilitate the uniform dispersion and stable composite formation of the $CaCO_3$ nanoparticles. Figure 1(b) illustrates the formation processes of pure $CaCO_3$ microparticles and $CaCO_3$/CNFs composite particles during spray drying.

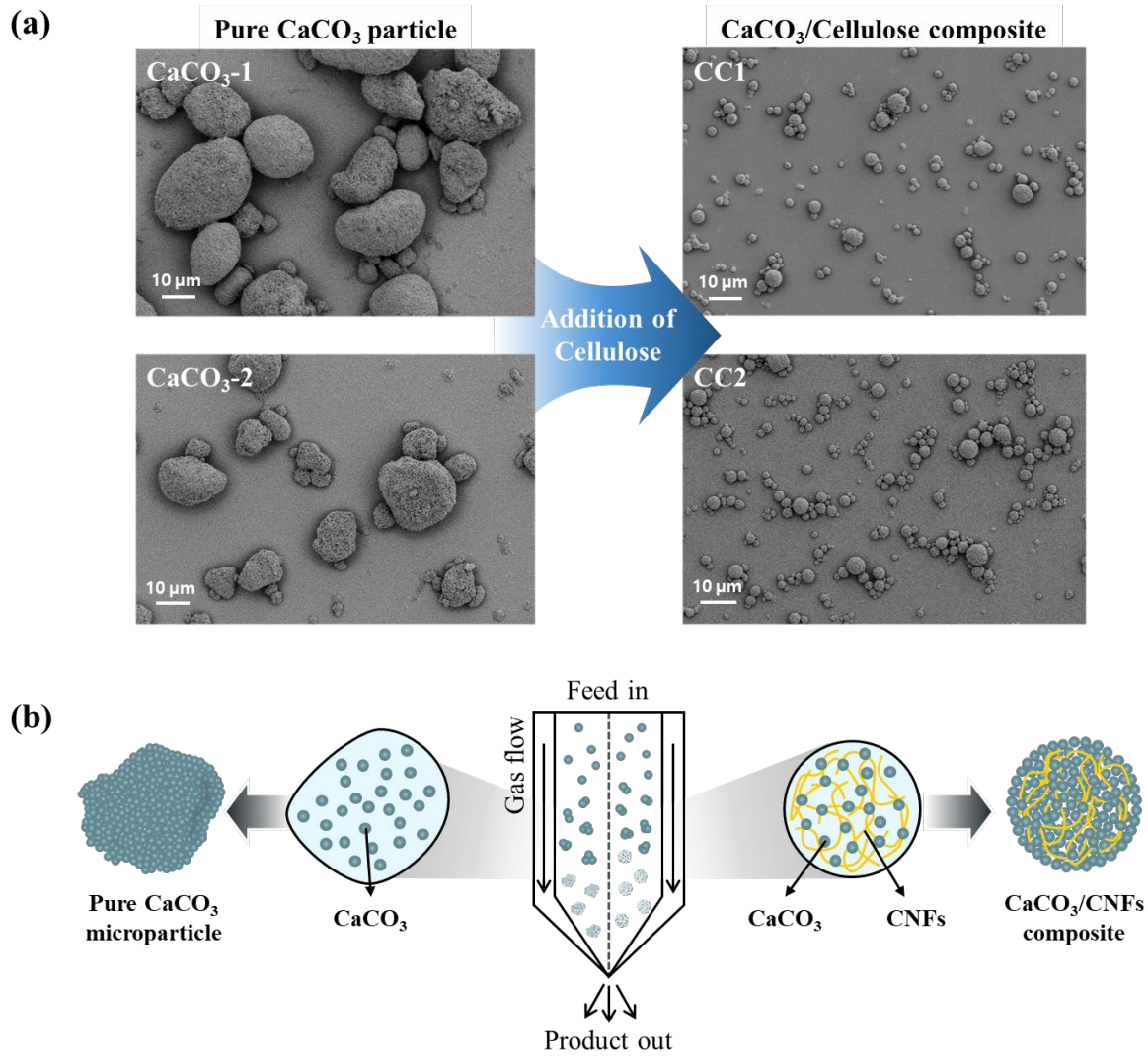

Figure 1. (a) FE-SEM images of spray-dried $CaCO_3$ microparticles and $CaCO_3$/CNFs composite particles with different feed rates. (b) Illustration of $CaCO_3$ microparticles and $CaCO_3$/CNFs composite particles manufacturing process via spray drying.

3.2. Surface morphology control of $CaCO_3$/CNFs composite particles

To investigate the effect of feed rate, a key parameter in the spray-drying process, on particle morphology, $CaCO_3$/CNFs composite particles were prepared at different feed rates. Figure 2 shows FE-SEM images of the surface and cross-section of $CaCO_3$/CNFs composite particles prepared at a high feed rate (8.3 mL/min) and low feed rate (2.8 mL/min). The CC1 particles prepared at the high feed rate exhibited a dense structure, whereas the CC2 particles formed at the low feed rate exhibited a mesoporous structure. This difference is attributed to the significant influence of the feed rate on the solvent evaporation dynamics within the droplets. At higher feed rates, a larger volume of liquid is introduced into the drying chamber, increasing the overall demand for the thermal energy required for solvent evaporation [10]. Consequently, the evaporation rate slows down, allowing $CaCO_3$ nanoparticles sufficient time to fill the voids within the three-dimensional CNFs network, ultimately resulting in a densely packed internal structure. Conversely, at lower feed rates, the droplet volume was smaller and required less thermal energy for evaporation. This led to a relatively higher drying gas temperature inside the chamber and a faster solvent evaporation rate. Rapid evaporation restricts the mobility of $CaCO_3$

nanoparticles within the CNFs network, limiting their ability to fill voids and leading to the formation of a mesoporous structure.

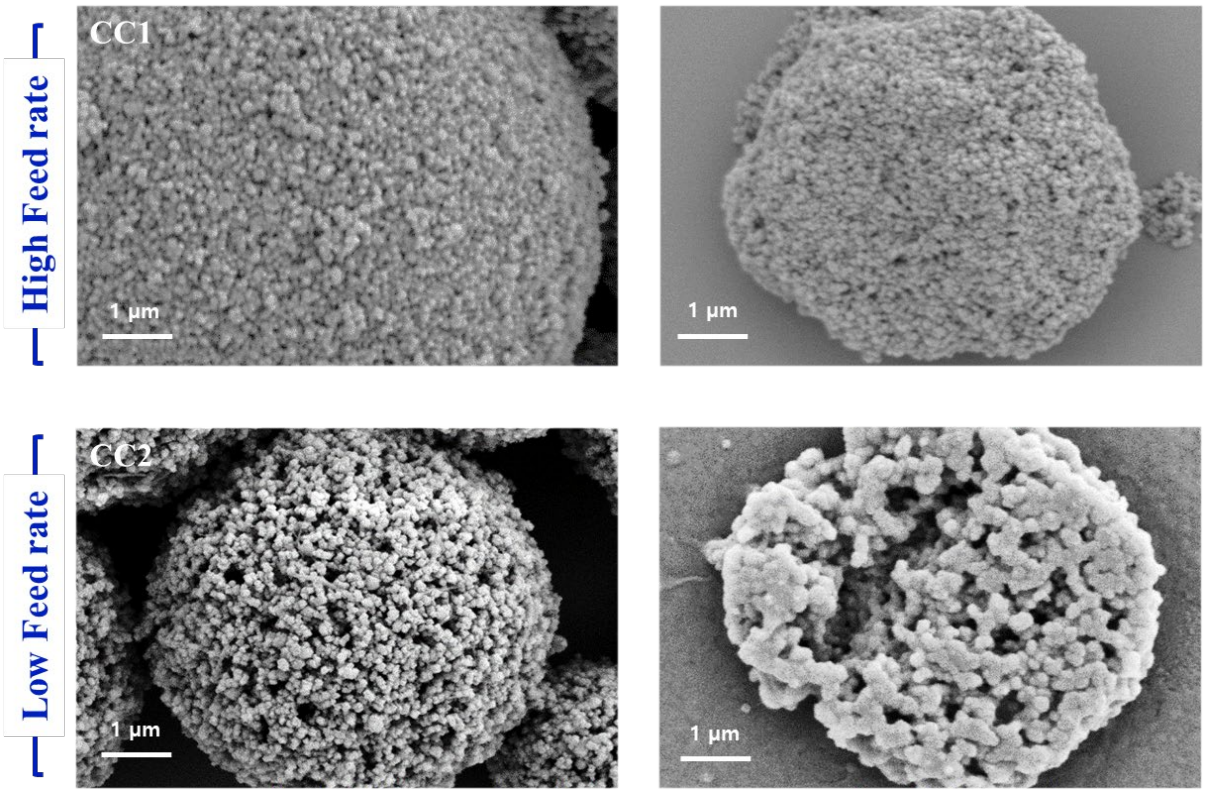

Figure 2. FE-SEM images of the surface and cross-section of spray-dried $CaCO_3$/CNFs composite particles at different feed rates.

4. Discussion

4.1. Optical performance evaluation of $CaCO_3$/CNFs composite particles

To evaluate the optical properties of the $CaCO_3$/CNFs composite particles, reflectance in the visible and near-infrared (NIR) regions was measured using an NIR spectrophotometer. Figure 3 presents a quantitative comparison of the particles based on the integrated areas of their reflectance spectra. The $CaCO_3$/CNFs composite particles exhibited approximately 57% higher reflectance in the visible region and approximately 24% higher reflectance in the near-infrared region compared to pure $CaCO_3$ microparticles. Notably, the CC2 composite particles prepared at a lower feed rate (2.8 mL/min) showed about 42% higher reflectance in the visible region and about 17% higher reflectance in the NIR region compared to the CC1 particles fabricated at a higher feed rate (8.3 mL/min). These results indicate that the $CaCO_3$/CNFs composite particles with a mesoporous structure exhibit superior light-reflecting performance compared to those with a dense structure. This is attributed to the rough and irregular surface morphology of the mesoporous particles, which promotes effective light-scattering and diffusion [11].

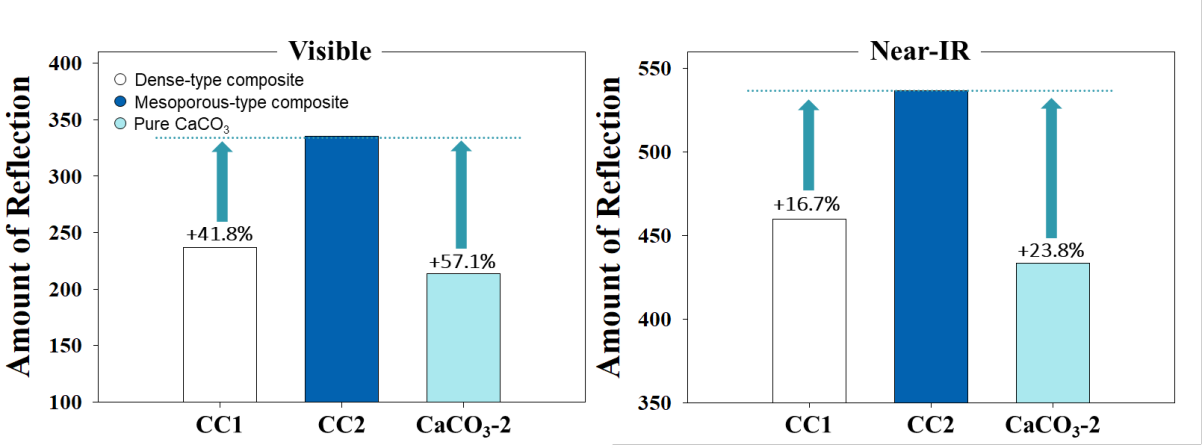

Figure 3. Integrated values of the spectral curves in the visible region (400–760 nm) and near-infrared region (760–1400 nm) of spray-dried $CaCO_3$ microparticles and $CaCO_3$/CNFs composite particles.

4.2. Soft-focus effect of $CaCO_3$/CNFs composite particles

To evaluate the soft-focus effect of the $CaCO_3$/CNFs composite particles, light scattering characteristics were measured using a goniophotometer and compared with spherical silica particles, which are widely used as soft-focus functional materials. Figure 4 presents the measured intensity of light reflected in the range of 0° to 180° after incident light was applied at a 45° angle to both spherical silica particles and spherical mesoporous $CaCO_3$/CNFs composite particles. The soft focus effect (SFF) can be defined as the ratio of the reflected light intensity at 65° ($\boldsymbol{Ld}$) to that at 135° ($\boldsymbol{Ls}$), expressed as $\boldsymbol{SFF} = \frac{\boldsymbol{Ld}}{\boldsymbol{Ls}}$. The spherical silica particles showed an SFF value of 0.183, whereas the spherical mesoporous $CaCO_3$/CNFs composite particles exhibited a significantly higher value of 0.518 [11]. The soft-focus effect is analogous to a blurring function that conceals visual imperfections. As the soft-focus effect increases, surface irregularities such as skin blemishes, wrinkles, and pores appear smoother and less noticeable, resulting in a more refined and even skin texture. Therefore, compared to spherical silica particles with a similar morphology, the $CaCO_3$/CNFs composite particles demonstrate a 183% enhancement in soft-focus performance, suggesting superior effectiveness in concealing skin imperfections.

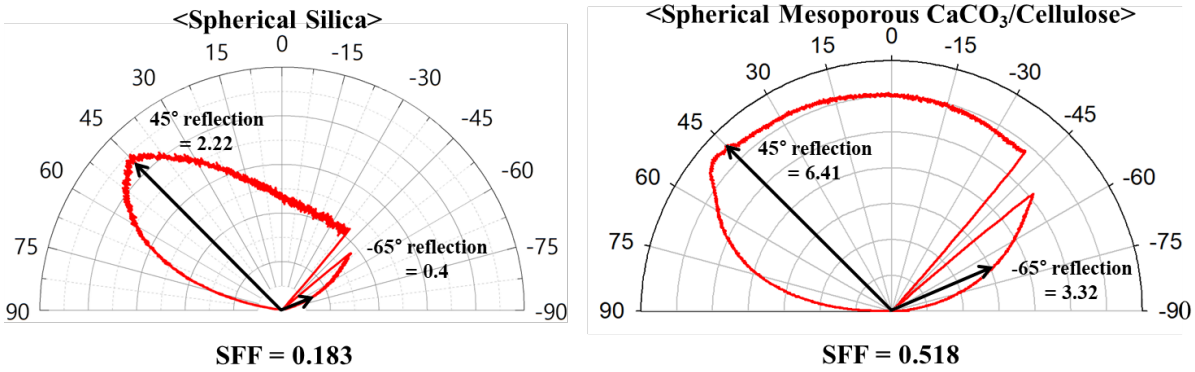

Figure 4. Light intensity distribution curves and soft-focus factor of spherical silica and spherical mesoporous $CaCO_3$/CNFs composite particles.

4.3. Water and oil repellency of $CaCO_3$/CNFs composite particles

To evaluate the water and oil repellency of the $CaCO_3$/CNFs composite particles, the contact angles were measured using DI water and mineral oil droplets. Figure 5 shows the formation of water and oil droplets on the surface of poly(methyl methacrylate) (PMMA) substrates coated with each type of particle. As both $CaCO_3$ and CNFs are hydrophilic materials, the pure $CaCO_3$ microparticles and the densely structured CC1 composite particles exhibited complete wetting behavior, with contact angles for water measuring 0°, indicating that the liquids spread easily on the surface. In contrast, the CC2 composite particles, which possess a mesoporous structure, exhibited reduced surface wettability owing to the air pockets formed between the particles. These air layers effectively inhibit liquid spreading, resulting in a relatively higher resistance to both water and oil [12]. As a result, the mesoporous $CaCO_3$/CNFs composite particles (CC2) exhibited a water contact angle of 25.23° and an oil contact angle of 53.27°.

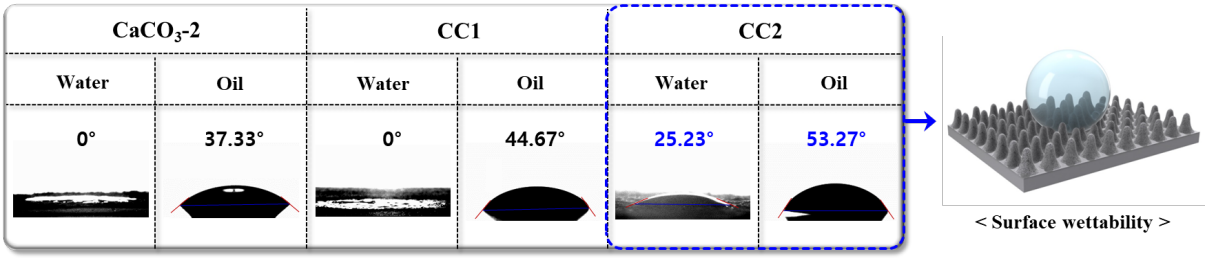

Figure 5. Water and oil contact angles of spray-dried $CaCO_3$ microparticles and $CaCO_3$/CNFs composite particles.

4.4. Particle hardness of $CaCO_3$/CNFs composite particles

To assess the mechanical properties of the $CaCO_3$/CNFs composite particles, nanoindentation testing was performed. Figure 6 is a graph showing the change in penetration depth according to the applied load on pure $CaCO_3$ microparticles and $CaCO_3$/CNFs composite particles, measured via nanoindentation. Based on the collected data, the hardness of the particles was calculated using the method proposed by Oliver and Pharr, as described by the following equation: $\boldsymbol{H_{IT}} = \frac{\boldsymbol{F_{max}}}{\boldsymbol{A_c}}$ where $\boldsymbol{H_{IT}}$ is the calculated hardness, $\boldsymbol{F_{max}}$ is the maximum applied load, and $\boldsymbol{A_c}$ is the projected contact area under the indenter tip at $\boldsymbol{F_{max}}$. The results showed that the $CaCO_3$/CNFs composite particles exhibited higher hardness than the pure $CaCO_3$ microparticles. This result is attributed to the incorporation of CNFs into the $CaCO_3$ matrix, which enhances intermolecular interactions and leads to the formation of a denser structure with improved mechanical strength capable of resisting plastic deformation. These findings suggest that CNFs function as a binder within the composite, thereby improving the mechanical integrity of the particles [13]. Furthermore, among the $CaCO_3$/CNFs composite particles, the densely structured CC1 particles demonstrated a 20.3% higher hardness than the mesoporous CC2 particles. This clearly indicates that the mechanical properties of the particles can be effectively controlled through a simple adjustment of the feed rate during the spray-drying process.

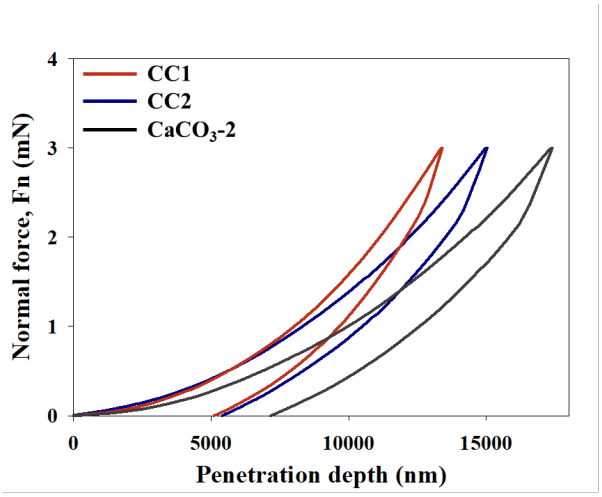

Sample No.	Morphology	H_{IT} (MPa)
CC1	Dense Spherical	1.121
CC2	Mesoporous Spherical	0.932
$CaCO_3$-2	Non-uniform	0.647

Figure 6. Nanoindentation depth curves of spray-dried $CaCO_3$ microparticles and $CaCO_3$/CNFs composite particles.

4.5. Spreadability of $CaCO_3$/CNFs composite particles

To evaluate the spreadability of the $CaCO_3$/CNFs composite particles, images of the particles applied to actual human skin were pixelated and converted into histograms. The standard deviation (SD) of pixel intensity was calculated, and the spreadability index (SI) was derived using the following equation: $\boldsymbol{Spreadability\ Index} = \frac{(\mathbf{50}-\boldsymbol{SD})}{\mathbf{50}} \times \mathbf{100}$. The results of the analysis are presented in Figure 7. The non-spherical pure $CaCO_3$ microparticles exhibited poor distribution on the skin surface, resulting in a relatively low SI value. In contrast, the spherical $CaCO_3$/CNFs composite particles showed a more uniform distribution, achieving a high SI value corresponding to the "good" category of spreadability. These findings indicate that when $CaCO_3$ nanoparticles are composited with CNFs and formed into a spherical shape, their adhesion to the skin and smoothness during application are significantly improved, thereby enhancing the overall spreadability performance.

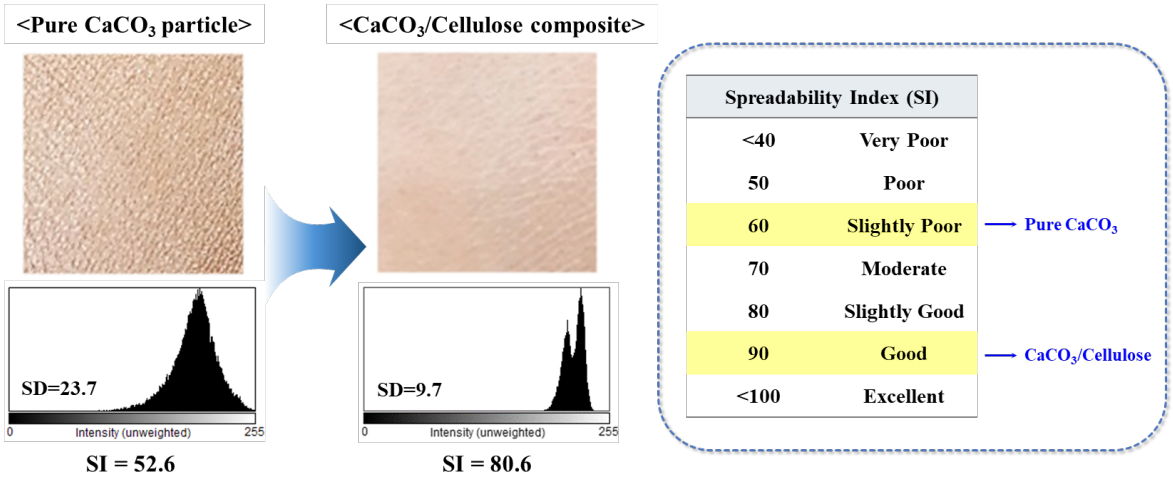

Figure 7. Image histogram and spreadability index of spray-dried $CaCO_3$ microparticles and $CaCO_3$/CNFs composite particles.

5. Conclusion

In this study, spherical $CaCO_3$/CNFs composite particles were successfully fabricated via co-spray drying of $CaCO_3$ nanoparticles and cellulose nanofibers (CNFs), which served as a

structural framework. During the fabrication process, electrostatic interactions between the abundant hydroxyl groups of CNFs and the oxygen atoms of carbonate ions enabled the effective binding of $CaCO_3$ nanoparticles within the cellulose network, thereby enhancing the structural stability of the composite particles. Furthermore, this study presents an innovative processing strategy by demonstrating that the morphology and porosity of the particles can be precisely controlled through the adjustment of the feed rate during spray drying. The mesoporous composite particles produced at a low feed rate exhibited superior optical properties and liquid repellency compared to the densely structured particles prepared at a high feed rate. Specifically, they achieved up to 47% and 17% higher reflectance in the visible and near-infrared regions, respectively, along with a 19% improvement in oil repellency. On the other hand, the dense composite particles showed 20.3% higher hardness than the hollow composite particles, demonstrating superior properties in terms of mechanical strength. Additionally, the $CaCO_3$/CNFs composite particles showed more uniform and smoother application behavior compared to pure $CaCO_3$ microparticles, resulting in significantly improved spreadability. Thus, the simple and sustainable manufacturing strategy presented in this study provides process excellence that can precisely control the structural and functional properties of the particles while utilizing cellulose as a functional building block and suggests the possibility of designing and applying multifunctional, plastic-free composite particles.

5. References.

1. Marto, J., Nunes, A., Martins, A. M., Carvalheira, J., Prazeres, P., Gonçalves, L., ... & Ribeiro, H. M. (2020). Pickering emulsions stabilized by calcium carbonate particles: A new topical formulation. Cosmetics, 7(3), 62.
2. Balabushevich, N. G., Lopez De Guerenu, A. V., Feoktistova, N. A., & Volodkin, D. (2015). Protein loading into porous CaCO3 microspheres: Adsorption equilibrium and bioactivity retention. Physical Chemistry Chemical Physics, 17(4), 2523–2530.
3. Wang, J., Chen, J. S., Zong, J. Y., Zhao, D., Li, F., Zhuo, R. X., & Cheng, S. X. (2010). Calcium carbonate/carboxymethyl chitosan hybrid microspheres and nanospheres for drug delivery. Journal of Physical Chemistry C, 114(44), 18940–18945.
4. Trushina, D. B., Sulyanov, S. N., Bukreeva, T. V., & Kovalchuk, M. V. (2015). Size control and structure features of spherical calcium carbonate particles. Crystallography Reports, 60(4), 570–577.
5. He, X., Lu, W., Sun, C., Khalesi, H., Mata, A., Andaleeb, R., & Fang, Y. (2021). Cellulose and cellulose derivatives: Different colloidal states and food-related applications. In Carbohydrate Polymers (Vol. 255). Elsevier Ltd.
6. Li, M. C., Wu, Q., Moon, R. J., Hubbe, M. A., & Bortner, M. J. (2021). Rheological Aspects of Cellulose Nanomaterials: Governing Factors and Emerging Applications. In Advanced Materials (Vol. 33, Issue 21). John Wiley and Sons Inc.
7. Salama, A. H. (2020). Spray drying as an advantageous strategy for enhancing pharmaceuticals bioavailability. In Drug Delivery and Translational Research (Vol. 10, Issue 1). Springer.
8. Dai, G., Zhang, J., Wang, X., Tan, H., & Rahman, Z. ur. (2022). Calcination and desulfurization characteristics of calcium carbonate in pressurized oxy-combustion. Energy, 261.

9. Sáenz Ezquerro, C., Laspalas, M., García Aznar, J. M., & Crespo Miñana, C. (2023). Monitoring interactions through molecular dynamics simulations: effect of calcium carbonate on the mechanical properties of cellulose composites. Cellulose, 30(2), 705–726.
10. Cortés-Rojas, D. F., Souza, C. R. F., & Oliveira, W. P. (2015). Optimization of spray drying conditions for production of Bidens pilosa L. dried extract. Chemical Engineering Research and Design, 93, 366–376.
11. Yoon, J., Lee, J. H., Lee, J. B., & Lee, J. H. (2020). Highly scattering hierarchical porous polymer microspheres with a high-refractive index inorganic surface for a soft-focus effect. Polymers, 12(10), 1–13.
12. Peng, Y., Jin, X., Zheng, Y., Han, D., Liu, K., & Jiang, L. (2017). Direct Imaging of Superwetting Behavior on Solid–Liquid–Vapor Triphase Interfaces. Advanced Materials, 29(45).
13. Upadhyay, R. K., & Kumar, A. (2019). Effect of particle weight concentration on the lubrication properties of graphene based epoxy composites. Colloids and Interface Science Communications, 33.